

Metalorganic vapor phase epitaxy growth, transmission electron microscopy, and magneto-optical spectroscopy of individual $\text{InAs}_x\text{P}_{1-x}/\text{Ga}_{0.5}\text{In}_{0.5}\text{P}$ quantum dots

O. Del Pozo-Zamudio,^{1,*} J. Puebla,^{1,2,†} A. Krysa,³ R. Toro,¹ A. M. Sanchez,⁴ R. Beanland,⁴ A. I. Tartakovskii,¹ M. S. Skolnick,¹ and E. A. Chekhovich^{1,‡}

¹*Department of Physics and Astronomy, University of Sheffield, Sheffield S3 7RH, United Kingdom*

²*Center for Emergent Matter Science, RIKEN, Wako, Saitama 351-0198, Japan*

³*Department of Electronic and Electrical Engineering, University of Sheffield, Sheffield S1 3JD, United Kingdom*

⁴*Department of Physics, University of Warwick, Coventry, CV4 7AL, United Kingdom*

(Received 4 May 2017; published 21 August 2017)

We report on growth and characterization of individual $\text{InAs}_x\text{P}_{1-x}/\text{GaInP}$ quantum dots with variable nominal As molar fraction. Magnetophotoluminescence experiments reveal quantum dot emission in a wide range from 1.3 to 1.8 eV, confirming successful incorporation of As into the quantum dots. Transmission electron microscopy reveals a core-cap structure of InAsP quantum dots with an InAs-rich core capped by an InP-rich layer. Inside the core, an average As molar fraction up to $x \approx 0.15$ is observed. The heavy-hole g factors are found to be strongly dependent on As molar fraction, while the electron g factors are close to the InP values. This suggests type-II carrier confinement in the studied InAsP dots with holes (electrons) localized in the core (cap) region. Finally, dynamic nuclear polarization is observed, which allows for further insight into structural properties using nuclear magnetic resonance.

DOI: [10.1103/PhysRevMaterials.1.034605](https://doi.org/10.1103/PhysRevMaterials.1.034605)

I. INTRODUCTION

Semiconductor quantum dots (QDs) play a crucial role in emerging semiconductor device technologies such as single photon sources and detectors, quantum memories, and logic gates [1]. Their electronic properties can be tailored by modifying their size and composition. For example, electronic properties of QDs can be engineered using ternary alloys. In this context, ternary $\text{III}_x\text{III}_{1-x}\text{V}$ QD systems have received most attention. Self-assembled Stranski-Krastanov $\text{In}_x\text{Ga}_{1-x}\text{As}/\text{GaAs}$ quantum dots are the most studied system, in which alloy composition and dot size can be modified to obtain a broad range of emission energies [2–4].

On the other hand, ternary $\text{III V}_x\text{V}_{1-x}$ Stranski-Krastanov QDs have not been studied in detail. $\text{InAs}_x\text{P}_{1-x}$ QDs grown by self-assembly in $\text{Ga}_{0.5}\text{In}_{0.5}\text{P}$ is the system considered in the present work. Due to the significant difference between the band gaps of InAs and $\text{Ga}_{0.5}\text{In}_{0.5}\text{P}$ (~ 1.5 eV at room temperature), a pronounced increase in confinement energy can be expected for InAsP/GaInP QDs compared to InP/GaInP QDs, favoring robust performance of QDs at elevated temperatures. The first report on Stranski-Krastanov growth of InAsP QDs in GaInP by metalorganic vapor phase epitaxy (MOVPE) was published by Vinokurov *et al.* [5]. However, no significant redshift of luminescence was observed compared to InP QDs which could have been a result of either inefficient As incorporation into QDs, or reduction of QD sizes under As incorporation. By contrast, Fuchi *et al.* have grown InAsP QDs using droplet heteroepitaxy technique and observed a significant

redshift and broadening of the ensemble QD emission with increased As fraction [6]. Ribeiro *et al.* reported experiments on InAsP/GaAs structures, where quantum dot emission at 77 K was found to be around 1.25 eV, which is above the emission energy of the InAs/GaAs QDs measured under the same conditions [7]. In the work of Ribeiro *et al.*, the electronic properties of InAsP/GaAs QDs were controlled by the PH_3 flux during the MOVPE process: as the flux was increased, the QD emission energy increased towards the InP QD energy [8]. In our work, we follow a similar approach and use the flux of AsH_3 to control the QD properties. Some recent examples of QD growth using ternary InAsP alloy also include demonstration of the InAsP QD lasers [9,10] and observation of ultraclean emission from InAsP QDs embedded in InP nanowires [11].

To the best of our knowledge, here we present the first report on growth, transmission electron microscopy and magneto-optical studies of individual InAsP/GaInP quantum dots that offer deeper confinement potential energies compared to the previously studied InP/GaInP and InAsP/GaAs QDs. Magnetophotoluminescence (magneto-PL) studies reveal the dependence of the electron and hole g factors on quantum dot emission energy that varies in a wide range between 1.3 and 1.8 eV. Such knowledge of the g factors is key for development of technologies that employ QD spins [12–14]. A combination of results from magneto-PL and transmission electronic microscopy (TEM) imaging suggests type-II carrier confinement in the studied $\text{InAs}_x\text{P}_{1-x}$ QDs for sufficiently large As molar fraction $x \sim 0.1$. Recently, type-II QDs have attracted considerable attention as potential candidates for efficient QD solar cells due to their increased carrier lifetime and suppressed Auger recombination [15–18].

The rest of the paper is organized as follows. The details of sample growth and experimental techniques are described in Sec. II. The experimental results are presented and discussed in Sec. III. Finally, in Sec. IV, we summarize the results of our work.

*Present address: Instituto de Investigación en Comunicación Óptica, Universidad Autónoma de San Luis Potosí, 78210 San Luis Potosí, S.L.P., Mexico; odelpozo@cactus.iico.uaslp.mx

†jorgeluis.pueblanunez@riken.jp

‡e.chekhovich@sheffield.ac.uk

II. SAMPLES AND EXPERIMENTAL METHODS

Our samples of ternary $\text{InAs}_x\text{P}_{1-x}$ QDs embedded into $\text{Ga}_{0.5}\text{In}_{0.5}\text{P}$ matrix were grown by low-pressure (150 Torr) MOVPE in a horizontal flow reactor, on (100) GaAs substrates with miscut angles of 3° towards (1 $\bar{1}$ 0). Trimethylgallium (TMGa) and trimethylindium (TMIn) were used as precursors for group-III elements, while arsine (AsH_3) and phosphine (PH_3) were used as precursors of group V. Hydrogen was used as a carrier gas. A GaAs buffer layer and a subsequent GaInP barrier were grown at 690°C . The growth rates were maintained at 0.76 nm/s for the GaAs buffer layers and GaInP barriers. QDs were deposited at a lower nominal growth rate of 0.11 nm/s. During the growth of the GaInP barriers and quantum dots the PH_3 flow was kept constant at 300 sccm, while the composition of the InAsP QDs was controlled by the flow rate of AsH_3 . Before the deposition of the QDs, the growth was halted, and the susceptor temperature was lowered to 650°C . The growth of the QDs included three steps: the first step involved deposition of a nominally binary InP for 1 s, this was followed by an InAsP deposition for 3 s during which arsine was introduced to the reactor, finally a nominally binary InP was grown again for 1 s. The sample with pure InP/GaInP dots (0 sccm arsine flux) was produced by growing InP for 5 s in a single step. In what follows, we label the samples by the arsine flux used during the dot growth.

In order to assess the nominal molar fractions of arsenic in the QDs grown with different AsH_3 flows, four control InAsP/InP superlattice (SL) samples were grown on InP substrates under the same growth conditions as for the QD structures. The growth times of the InAsP layers were 5 or 10 s and the total growth times of one complete SL period were 60 s or 120 s, respectively. The SL structures were examined by means of x-ray diffractometry as described in Ref. [10]. The molar fractions were derived from the position of the zero order SL peak with respect to the peak from the InP substrate. The resulting arsenic molar fractions in the InAsP layers are $x = 0.06, 0.072, 0.084,$ and 0.108 for AsH_3 flows of 5.9, 10.6, 16.7, and 20.2 sccm, respectively. These values can be used as reference when examining incorporation of As into the quantum dots.

Optical characterization of the QDs was carried out using a microphotoluminescence (μPL) setup equipped with a confocal low-temperature optical microscope system. An external magnetic field up to 10 T parallel (Faraday geometry) or perpendicular (Voigt geometry) to the sample growth axis was applied using a superconducting magnet. In most experiments PL was excited using either a HeNe laser ($E_{\text{exc}} = 1.96$ eV) or a diode laser ($E_{\text{exc}} = 1.88$ eV), with additional diode lasers ($E_{\text{exc}} = 1.80$ and 1.53 eV) used for experiments on nuclear spin effects. Photoluminescence signal was collected with a 0.85 m double spectrometer and a liquid nitrogen cooled charge coupled device (CCD). All optical spectroscopy experiments were carried out at a sample temperature of 4.2 K. Electron microscopy characterization of the QDs presented in Sec. III A was conducted using both conventional and aberration-corrected scanning high-resolution transmission electron microscopy (TEM/STEM), details are given in Ref. [9].

III. RESULTS AND DISCUSSION

A. Transmission electron microscopy

We carried out transmission electron microscopy studies in order to examine the morphology and chemical composition of the quantum dots. Figure 1(a) shows a conventional TEM image taken under 002 dark field conditions on a sample grown without As (0 sccm). Contrast in these images is sensitive to the difference in the mean atomic number of the group III and V superlattices. Two types of InP/GaInP quantum dots are observed: large pyramid-shaped dots (e.g., left side of the image) and smaller disk shaped dots (e.g., right side of the image). Further examples of disk-shaped InP/GaInP dots are shown in Fig. 1(b). Similar 002 dark field TEM images of InAsP/GaInP dots (20.2-sccm sample) are shown in Fig. 1(c). It is apparent that these InAsP dots are pyramid shaped and have smaller lateral dimensions of ~ 40 nm as opposed to ~ 80 nm for both types of the InP dots in Figs. 1(a) and 1(b).

In order to examine the chemical composition, further studies on InAsP/GaInP dots (20.2-sccm sample) were conducted using aberration-corrected scanning TEM (AC-STEM). Representative images taken under annular dark field (ADF) conditions are shown in Figs. 1(d) and 1(e). In these images, brighter areas correspond to elements with larger atomic number Z . It is apparent that a typical InAsP dot consists of a core containing heavy elements covered by a cap of lighter elements. The images are aligned with the (001) planes horizontal, showing the QDs have formed preferentially in local steepenings of the 3° offcut surface. Cu-Pt type ordering in the InGaP matrix is evident from the fast Fourier transform (FFT) shown in the top right box in Fig. 1(e); no such ordering is observed in the QD core or cap (FFT in the bottom left box).

In order to quantify segregation of elements inside InAsP QDs, we have performed energy-dispersive x-ray analysis (EDX): the fractions of all chemical elements measured in a scan along the A \rightarrow B line in Fig. 1(e) are shown in Fig. 1(f) by the solid lines. The observed structure is significantly different from the nominal sequence of growth layers (1 s InP) - (3 s InAsP) - (1 s InP). Substitution of Ga atoms by heavier In atoms is observed predominantly in the top part of the dot [9 nm $\lesssim z \lesssim 16$ nm in Fig. 1(f)]—this is in agreement with earlier observations of increased In concentration at the top of the dot in InGaAs/GaAs structures [19,20]. By contrast, substitution of P atoms with As atoms is dominant at the bottom of the dot [6 nm $\lesssim z \lesssim 13$ nm in Fig. 1(f)] and can be related to As/P exchange reaction observed previously in InAs/InP quantum dots [21]. Substitution of the lighter P and Ga atoms by the heavier As and In atoms increases the lattice constant a_0 . In order to examine the contributions of As and In segregation we have calculated the nominal (unaffected by strain) a_0 using the measured composition shown by the solid lines in Fig. 1(f) and the known quaternary InGaAsP alloy parameters [22]. The calculated a_0 is shown by the dashed line in Fig. 1(f) and is seen to reach its maximum approximately at the middle of the dot ($z \approx 11$ nm). However, the curve is asymmetric: a_0 is on average larger in the top part of the dot, which is in agreement with earlier findings [19] that the segregation of the material with a larger lattice constant at the apex of the dot

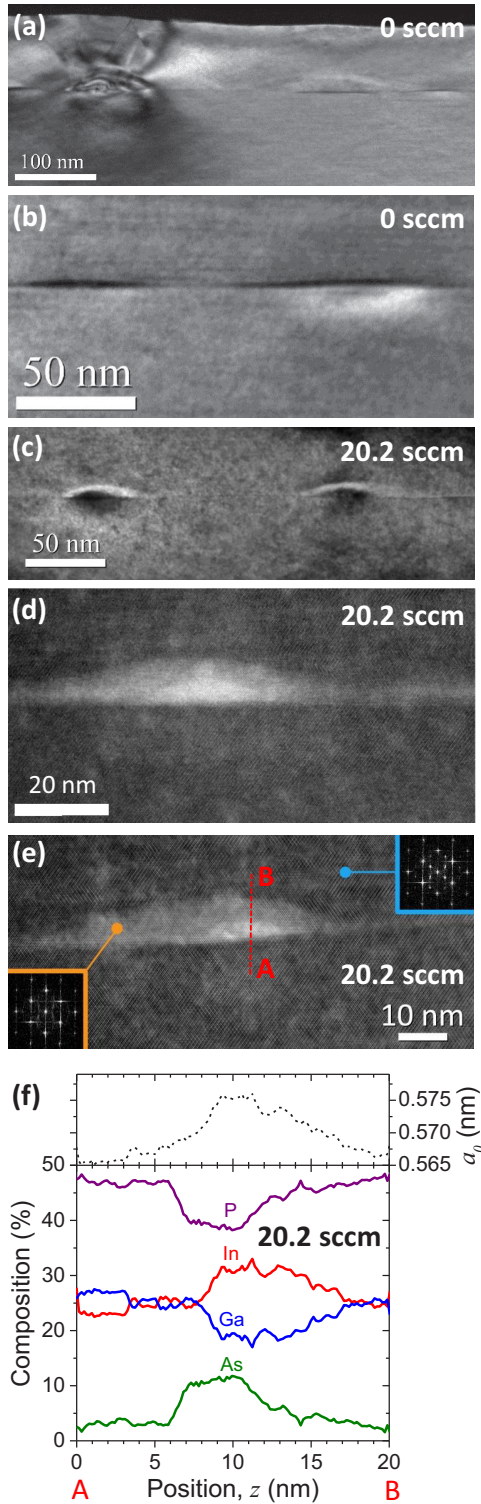


FIG. 1. Transmission electron microscopy (TEM) of InP/GaInP quantum dots in a 0-sccm sample [(a) and (b)] and InAsP/GaInP dots in a 20.2-sccm sample [(c)–(f)]. Images (a)–(c) were taken under 002 dark field conditions. Images (d) and (e) were obtained using scanning TEM under annular dark field (ADF) conditions. Insets in (e) show Fourier transforms revealing Cu-Pt type ordering in the GaInP barrier, not observed in a quantum dot. (f) Results of energy-dispersive x-ray analysis: fractions of all chemical elements measured along the A \rightarrow B line in (e) are shown by the solid lines. The dashed line shows the nominal lattice constant a_0 calculated from chemical composition.

is favored by the reduction of the elastic energy. Taking the arsenic/phosphorus ratio in Fig. 1(f) we can estimate the peak arsenic fraction to be $x \approx 0.24$. Averaging over the height of the dot ($6 \text{ nm} \lesssim z \lesssim 17 \text{ nm}$) we estimate the mean arsenic fraction to be $x \approx 0.15$, which is in qualitative agreement with $x = 0.108$ derived from x-ray diffractometry on the reference superlattice sample grown with the same arsine flow rate of 20.2 sccm.

In summary, TEM imaging shows that the sample growth with AsH_3 flow results in arsenic incorporation into quantum dots. The resulting InAsP dots have notably smaller lateral dimensions than InP dots and exhibit a core-cap structure, resembling the core-shell structure of colloidal dots [15]. As we show below, these findings agree with the measurements of the diamagnetic shifts and carrier g factors in individual dots. Furthermore, we present experimental results that point to type-II confinement in such core-cap geometry with electrons localized in the InP-rich cap and holes occupying the InAs-rich core.

B. Effect of arsenic incorporation on quantum dot photoluminescence

Figure 2 shows μPL spectra of six InAsP QD samples grown with different nominal As concentrations. The spectra were measured in a wide range of energies (1.3–1.85 eV). Relative concentrations of As are given in terms of AsH_3 flux in standard cubic centimeters per minute (sccm) on the left side of the graph. The top spectrum (black line) shows QD emission of the sample without arsenic (InP/GaInP). The spectrum is similar to those reported previously [24]: the sharp peaks at 1.67–1.8 eV are attributed to the disk shaped quantum dots [see Fig. 1(b)], while broad emission features centered at 1.65 eV most likely originate from the large pyramidal quantum dots [see Fig. 1(a)]. When AsH_3 flux is increased (spectra from top to bottom), the spectral range of the quantum dot emission peaks progressively widens, extending below the GaAs substrate emission at 1.52 eV for As concentrations above 2.9 sccm. The samples with the largest AsH_3 flux (20.2 and 50 sccm) exhibit single-dot emission in a wide range spanning from 1.3 to 1.8 eV. Importantly, there are quantum dots with emission energies below the bulk band gap of InP (1.421 eV at $T = 4.2 \text{ K}$). Such pronounced shift of PL emission to lower energies is a clear sign that arsenic is incorporated into quantum dots.

It follows from the spectra of Fig. 2, that quantum dot PL intensity decreases with increasing arsenic concentration. As we discuss later, such behavior could be a result of the transition from type-I to type-II carrier confinement for quantum dots with high arsenic concentration. Even for the highest As fraction, the typical luminescence linewidths of the studied QDs are less than $\sim 50 \mu\text{eV}$ suggesting that As incorporation does not deteriorate the optical quality of the InAsP/InP dots.

C. Magnetophotoluminescence spectroscopy

In this section, we present results of μPL spectroscopy in external magnetic fields for quantum dot samples with different As concentration. Using these results, we explore

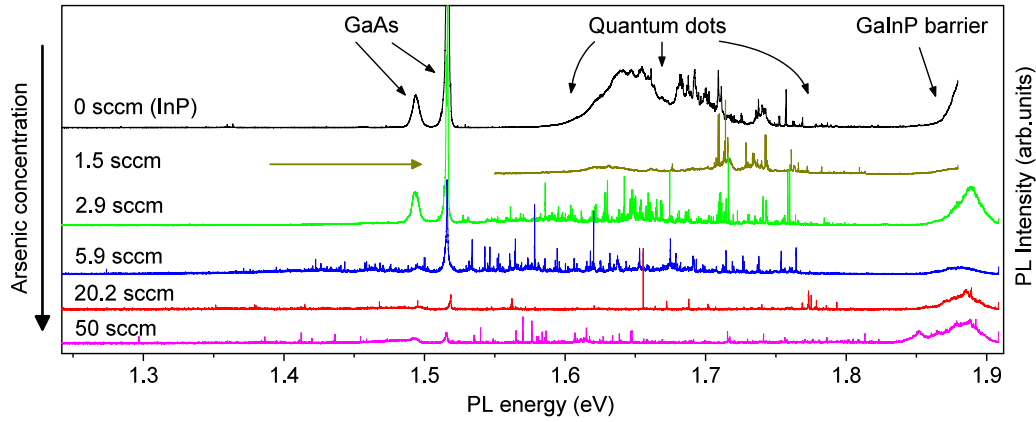


FIG. 2. Low-temperature photoluminescence spectra of six InAsP/GaInP QD samples with different nominal As concentration measured under HeNe laser excitation ($E_{exc} = 1.96$ eV). The AsH_3 flux used for the growth of each sample is given in standard cubic centimeters per minute (sccm). Emission from a GaAs substrate, quantum dots, and GaInP barriers can be seen in the spectra. Increased AsH_3 flux results in a pronounced redshifting of the emission, signifying incorporation of As into quantum dots. Such incorporation is accompanied by reduction of the quantum dot luminescence intensity as well as suppression of the GaAs emission, which is attributed to absorption by the quantum dot layer. The variations in the GaInP emission energy and reduction with respect to the values for a disordered bulk GaInP (~ 1.99 eV, Ref. [23]) are likely due to Cu-Pt ordering, in agreement with the TEM results in shown Fig. 1(e).

how electron and hole states are modified by incorporation of As into InP QDs. As we show, such studies also provide information on the chemical composition and structure of the InAsP QDs, complementary to the TEM imaging.

1. Derivation of the quantum dot charge states and g factors

We first present magneto-PL spectroscopy data, which reveals information on the charge states of the QDs. Two different geometries were used in our measurements: in Faraday (Voigt) geometry magnetic field is applied parallel (perpendicular) to the sample growth axis $B \parallel z$ ($B \perp z$). Figure 3(a) shows PL spectra of a single quantum dot in a sample with large As concentration (20.2 sccm) detected in two circular polarizations in Faraday geometry and in two orthogonal linear polarizations in Voigt geometry. Magnetic

field dependence of the spectral positions of the peaks observed in Fig. 3(a) is shown in Fig. 3(b) by the symbols. Zeeman splitting and diamagnetic shift are observed both for $B \parallel z$ and $B \perp z$. In Faraday geometry, the QD emission line splits into a circularly polarized (σ^+ and σ^-) doublet, whereas in Voigt geometry a quadruplet of linearly polarized (π_1 and π_2) lines is observed.

In order to describe the dependence of the PL peak energies on magnetic field B we use the following equations [25]:

$$E_F(B) = E_0 + \kappa_F B^2 \pm \frac{1}{2} g_X \mu_B B, \tag{1}$$

$$E_V(B) = E_0 + \kappa_V B^2 + \frac{1}{2} \mu_B B (\pm g_{h,\perp} \pm g_e), \tag{2}$$

where E_0 is the emission energy at $B = 0$, μ_B the Bohr magneton, κ_F and κ_V are the diamagnetic shifts in Faraday and

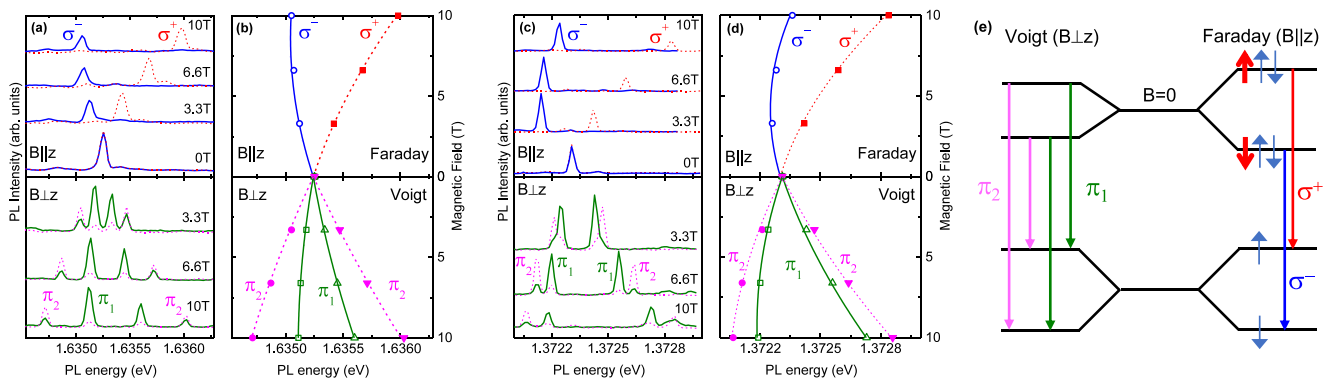


FIG. 3. (a) Typical magnetic field dependence of PL spectra from an individual InAsP/GaInP quantum dot in a 20.2-sccm sample measured at 4.2 K under a nonresonant excitation in σ^+ and σ^- polarized detection in Faraday geometry (top part $B \parallel z$) and in orthogonal π_1, π_2 linearly polarized detection in Voigt geometry (bottom part $B \perp z$). The spectral patterns observed in Voigt geometry reveal that photoluminescence originates from singly charged dots [25]. (b) Energies of the peaks derived from the spectra in (a) vs external magnetic field (symbols). Solid lines show fitting with Eqs. (1) and (2) allowing g factors and exciton diamagnetic shifts to be determined. (c) Magnetic field PL dependence of another QD from the same sample emitting at lower energy. (d) PL peak energies from (c) and fitting. (e) Schematic diagram of the spin levels and allowed optical transitions in a negatively charged InAsP quantum dot in Faraday and Voigt configurations. Electrons (holes) are shown with thin (thick) arrows representing spin-up and spin-down states.

Voigt geometries, respectively, $g_X = (g_{h,\parallel} - g_e)$ is the exciton g factor in Faraday geometry, $g_{h,\parallel}$ ($g_{h,\perp}$) is the heavy-hole g factor along (perpendicular to) the sample growth axis, and electron g factor g_e is assumed to be isotropic. We performed simultaneous least-square fitting of the data measured in Faraday (Voigt) geometry to Eq. (1) [Eq. (2)]. The fitting results for the data in Figs. 3(a) and 3(b) are shown by the lines in Fig. 3(b) and yield $g_X = +1.592$, $g_{h,\parallel} = +3.175$, $g_e = +1.58$, $|g_{h,\perp}| = 0.737$, $\kappa_F = 2.67 \mu\text{eV}/\text{T}^2$, and $\kappa_V = 1.12 \mu\text{eV}/\text{T}^2$. The same analysis is presented in Figs. 3(c) and 3(d) for another single dot from the same sample emitting at lower energy. Once again the data is well described by Eqs. (1) and (2) but with notable difference in g factors and diamagnetic shifts, which is discussed in more detail in Secs. III C 2 and III C 3. Due to the \pm signs in Eqs. (1) and (2) there is a potential ambiguity in the signs of the fitted g factors. However, the signs of $g_{h,\parallel}$ and g_e are reliably established by comparing with the previous studies on neutral InP/GaInP quantum dots [26] and bulk InP [27]. By contrast, the sign of $g_{h,\perp}$ is not defined and only the absolute value $|g_{h,\perp}|$ can be found from the fitting.

The patterns of the spectral components in Figs. 3(a) and 3(c) as well as their good description within the model of Eqs. (1) and (2) prove that the observed QD emission peaks arise from singly-charged quantum dots [25]. In particular, in Voigt geometry, all four peaks maintain similar intensities and converge to the same energy in the limit of $B \rightarrow 0$, as opposed to the behavior of the “dark” excitons in neutral quantum dots [25,28]. The origin of two (four) spectral peaks in Faraday (Voigt) geometry is illustrated in Fig. 3(c) where spin states and optical transitions are shown schematically for a negatively charged exciton.

All narrow spectral peaks that have been examined, exhibit similar trion behavior in all of the studied samples. This suggests that all of the studied dots emit from a charged state, which can be ascribed to the combined effect of the background doping and optical excitation above the GaInP barrier band gap. Distinguishing between positively and negatively singly charged dots using PL spectroscopy alone is difficult. However, we note that high magnetic field ($B = 10$ T) applied in Faraday geometry leads to unequal intensities of the two Zeeman PL components—a sign of relaxation between electron or hole spin Zeeman levels. We observe dots where both high- and low-energy peak becomes dominant in high field [compare Figs. 3(a) and 3(c)], suggesting that both positively and negatively charged quantum dots are encountered in the studied samples.

2. Effect of arsenic incorporation on diamagnetic shifts

Measurements of exciton diamagnetic shifts and exciton g factors (g_X) have been carried out for ~ 120 QDs that have been selected for relatively bright PL and narrow linewidths in five samples with different As concentration (AsH₃ fluxes between 0–20.2 sccm). Figures 4(a) and 4(b) show the exciton diamagnetic shifts κ_F and κ_V measured in Faraday and Voigt geometries, respectively. Measurements of κ_F and κ_V allow the effects of arsenic incorporation on quantum dot size and shape to be examined. The diamagnetic shift κ is related to the radius of the exciton wave function r_X in the plane perpendicular to

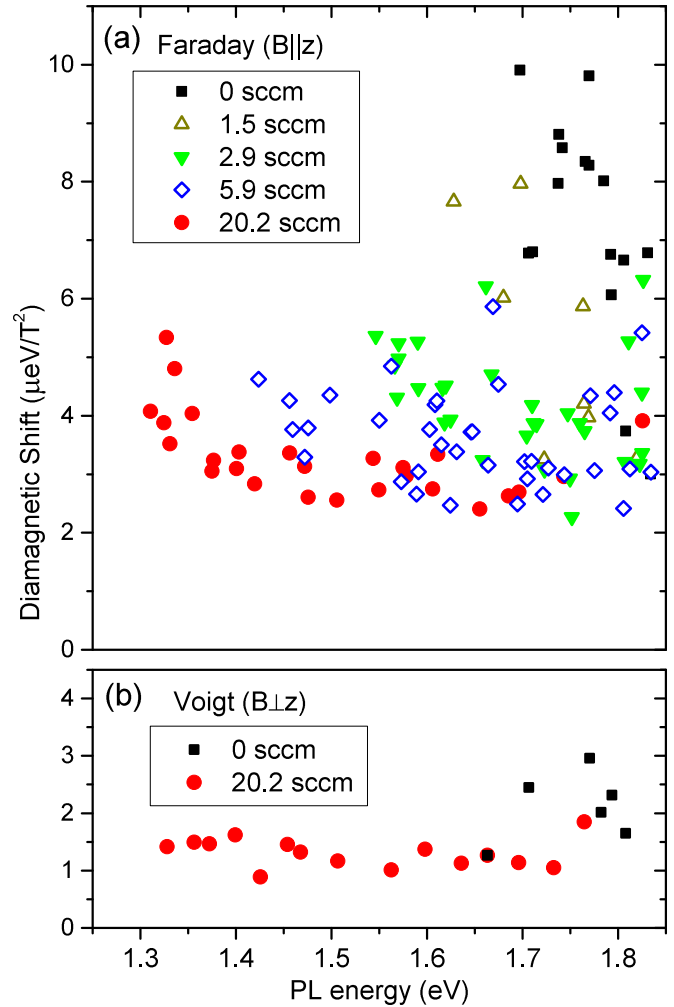


FIG. 4. Diamagnetic shifts κ as a function of emission energy measured in Faraday (a) and Voigt (b) geometries for a large number of individual InAsP quantum dots in five samples with different arsenic concentration (determined by AsH₃ flux during the growth, ranging between 0 and 20.2 sccm). There is a pronounced reduction of κ_F with increasing As fraction observed in Faraday geometry, revealing the reduction of the lateral QD sizes induced by As incorporation.

the external magnetic field by the following equation [29]:

$$\kappa = \frac{e^2}{8\mu} r_X^2, \quad (3)$$

where e is the electron charge and μ is the reduced exciton mass.

It can be seen in Fig. 4(a) that the largest diamagnetic shifts in Faraday geometry $\kappa_F \sim 8 \mu\text{eV}/\text{T}^2$ are observed for pure InP dots (0-sccm sample). Increased arsenic concentration results in reduced κ_F for the dots emitting at the same energies. This trend in diamagnetic shifts suggests that incorporation of arsenic into InAsP quantum dots results in reduction of their lateral dimensions. Such conclusion agrees with the TEM results presented in Sec. III A. Furthermore in the sample with large As fraction (20.2 sccm) κ_F tends to increase for quantum dots with smaller emission energy suggesting their increased lateral dimensions. The diamagnetic shifts in Voigt geometry

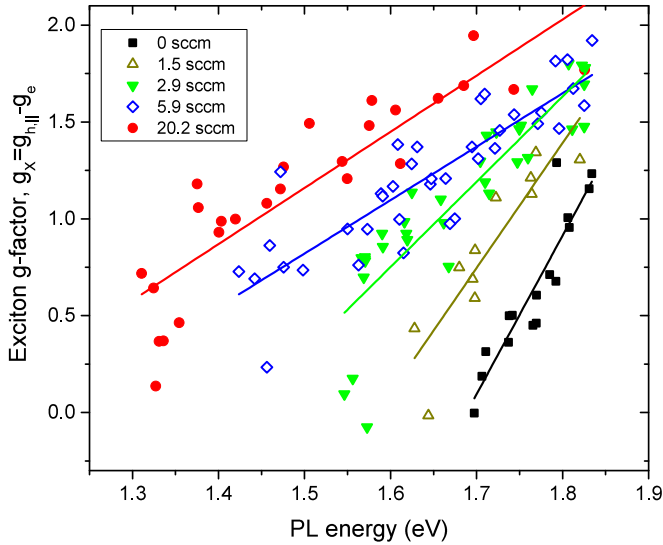


FIG. 5. Exciton g factors g_X measured in Faraday configuration as a function of emission energy for a set of quantum dots in five samples with different As concentration. Solid lines are linear fits (see fitted parameters in Table I).

κ_V presented in Fig. 4(b) are notably smaller than κ_F agreeing with the disk-shape nature of the dots revealed by the TEM.

3. Effect of arsenic incorporation on g factors and analysis of carrier confinement

In order to gain deeper insight into the spin properties of InAsP QDs, we extract the magnitudes of g factors for samples with different arsenic content. As we show below, these results provide useful information about quantum dot composition and structure and point to a type-II carrier confinement.

The symbols in Fig. 5 show the out-of-plane exciton g factors g_X measured in Faraday geometry as a function of the QD ground-state emission energy in five samples. Linear fits are plotted by the lines to visualize the trends in exciton g factors for samples with different As compositions; the fitting parameters are listed in Table I. It can be seen from Fig. 5 that increased AsH_3 flux leads to a systematic increase in the exciton g factors at all energies E where QD luminescence is observed. Furthermore, the slopes m of the $g_X(E)$ dependencies decrease for large As concentration. These pronounced variations in g_X signify the change in the chemical composition in the QD volume where exciton wave

TABLE I. Parameters derived from fitting the exciton g factors using a linear model $g_X(E) = m(E - 1.8 \text{ eV}) + g_X(1.8 \text{ eV})$, where E is the QD ground-state emission energy (the fits are shown by the lines in Figure 5).

Sample	m (eV^{-1})	g_X at $E = 1.8 \text{ eV}$
0 sccm	8.18567	0.904
1.5 sccm	6.459	1.381
2.9 sccm	4.400	1.640
5.9 sccm	2.758	1.640
20.2 sccm	2.899	2.012

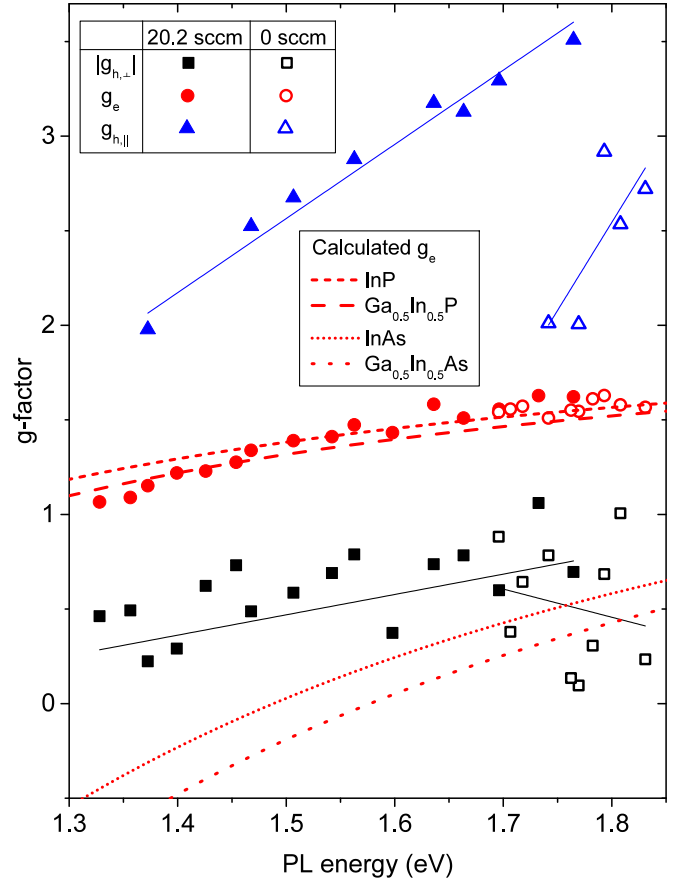


FIG. 6. Electron (g_e , circles), out-of-plane heavy hole ($g_{h,||}$, triangles), and in-plane heavy-hole ($g_{h,\perp}$, squares) g factors measured for InP/GaInP quantum dots (0-sccm sample, open symbols) and InAsP/GaInP dots (20.2-sccm sample, solid symbols) shown as a function of the dot photoluminescence energy. Thin solid lines show linear fits that can be used as a guide to an eye. Electron g factors calculated using Eq. (4) are shown for the cases of InP (short dashed line), $\text{Ga}_{0.5}\text{In}_{0.5}\text{P}$ (long dashed line), InAs (short dotted line), and $\text{Ga}_{0.5}\text{In}_{0.5}\text{As}$ (long dotted line). A very good agreement between experimental g_e values and the theory for the phosphide compounds is found, suggesting that electron and hole wave functions are spatially separated with electrons localized in the phosphorus-rich areas of the dots.

function is localized and thus confirm successful incorporation of As into the dots.

In order to gain further insight, we examine the contributions of the electron and hole g factors to the variation of the exciton g_X observed in Fig. 5. For this purpose we focus on two samples with zero and large (20.2 sccm) arsenic concentration and conduct systematic magneto-PL experiments where the same dots are measured both in Faraday and Voigt geometry allowing electron and hole g factors to be derived as described in Sec. III C 1. Figure 6 shows the extracted g factors for the 0-sccm sample (open symbols) and the 20.2-sccm sample (solid symbols). The thin solid lines are linear fits, which can be used as guides to an eye. We first note the large spread in the $|g_{h,\perp}|$ values, which is expected since heavy hole in-plane g factors depend strongly on the anisotropy of shape and strain of each particular dot [25]. The results for the out-of-plane

heavy hole g factors $g_{h,\parallel}$ and for the electron g factors g_e are more robust and show a striking difference: while g_e values follow the same trend for both samples, there is a pronounced deviation in $g_{h,\parallel}$ values. It is thus evident that the heavy holes are the most sensitive to incorporation of arsenic into the InAsP dots, whereas electrons have similar properties in structures with and without arsenic.

For quantitative analysis, we use the result of Roth *et al.* [30] that electron g factor is determined mainly by the band gap of the semiconductor. While it was derived originally for bulk materials, this result has been extended successfully to quantum wells and quantum dots [31–33]. Thus we write for the electron g factor:

$$g_e = 2 - \frac{2E_P \Delta}{3E_g(E_g + \Delta)}, \quad (4)$$

where E_g is the band gap, Δ is the spin-orbit splitting and E_P is the Kane energy parameter. (We adopt the Δ and E_P values from Ref. [34] and use linear interpolation for ternary alloys.) Equation (4) is plotted in Fig. 6 by the dashed lines for InP and $\text{Ga}_{0.5}\text{In}_{0.5}\text{P}$ and by the dotted lines for InAs and $\text{Ga}_{0.5}\text{In}_{0.5}\text{As}$. The simple theoretical equation is in excellent agreement with the experimental g_e values if we assume pure phosphide parameters (regardless of the degree of In/Ga mixing between the dot and the $\text{Ga}_{0.5}\text{In}_{0.5}\text{P}$ barrier). We thus conclude that both in the InAsP and InP dots the electron behaves as if the dot is arsenic-free, with small deviation developing only for the dots with the lowest ground-state energies. While $g_{h,\parallel}$ can not be calculated in a simple way, it is generally proportional to the κ and q parameters of the valence band [35] and can thus be expected to be larger for InAs than for InP. Therefore the increased values of $g_{h,\parallel}$ in the 20.2-sccm sample compared to the 0-sccm sample (Fig. 6) are attributed to the increased fraction of arsenic “sampled” by the hole wave function in the InAsP dots. To summarize, our observations strongly suggest that electrons and holes are localized in spatially separated parts of the quantum dot.

We propose the following interpretation that agrees with the observed g -factor values, the reduced luminescence intensity of QDs with large As concentration, and the TEM results of Sec. III A: the growth conditions favor the formation of core-cap QDs where InP-rich cap region localizes the electron and is separated from the InAs-rich core region where the hole is predominantly localized. Such spatial separation of electrons and holes may give rise to type-II QD behavior. This conclusion is nontrivial since electronic band alignment at InAsP/InP interface is expected to be of type-I (Ref. [34]). The most likely explanation is that large inhomogeneous strain characteristic of self-assembled QDs can lead to significant shift in energy levels [36] and can be responsible for the type-II band alignment.

Recently, type-II QDs have received increased attention as promising candidates for QD solar cell applications, where spatial separation of electrons and holes reduces spontaneous recombination and favors carrier extraction. Moreover, the structures studied here exhibit InAsP QDs with a broad range of the band-gap energies (from ~ 1.3 to ~ 1.8 eV), which could be advantageous for light conversion efficiency.

D. Optical control of the quantum dot nuclear spins

All isotopes of the elements present in the studied InAsP/GaInP quantum dots have non-zero nuclear spins, as a result electron-nuclear interactions are significant [37–39]. Using circularly polarized optical excitation it is possible to inject spin-polarized electrons into quantum dots. Spin-polarized electrons can then transfer their polarization to one of the $\sim 10^5$ nuclear spins of the dot via electron-nuclear hyperfine interaction. Repeated optical recombination and re-excitation of the spin-polarized electrons can then lead to substantial polarization of the quantum dot nuclear spin ensemble with polarizations degrees as large as 80% (Ref. [40]). Such dynamic nuclear polarization (DNP) process has been reported previously for different types of quantum dots [40–43] including InP/GaInP quantum dots [26,28,44–46]. Here we extend these studies to InAsP/GaInP quantum dots.

The measurements were conducted on the 20.2-sccm sample in an external magnetic field parallel to the sample growth direction (Faraday geometry). Magnetic field splits the QD emission peak into a Zeeman doublet [see Figs. 3(a) and 3(c)]. Since the two peaks of the spectral doublet originate from electron states with opposite spins [see Fig. 3(d)] the onset of the nuclear spin polarization results in a hyperfine (Overhauser) shift, i.e., in an increase or a decrease of the Zeeman splitting ΔE depending on the direction of the effective nuclear field. (Here, for simplicity, we neglect the interaction of the hole spin with the nuclei since its contribution is at least ten times smaller than that of the electron [46,47].)

The change in ΔE induced by the DNP can be detected in the PL spectra as demonstrated in Fig. 7 where two

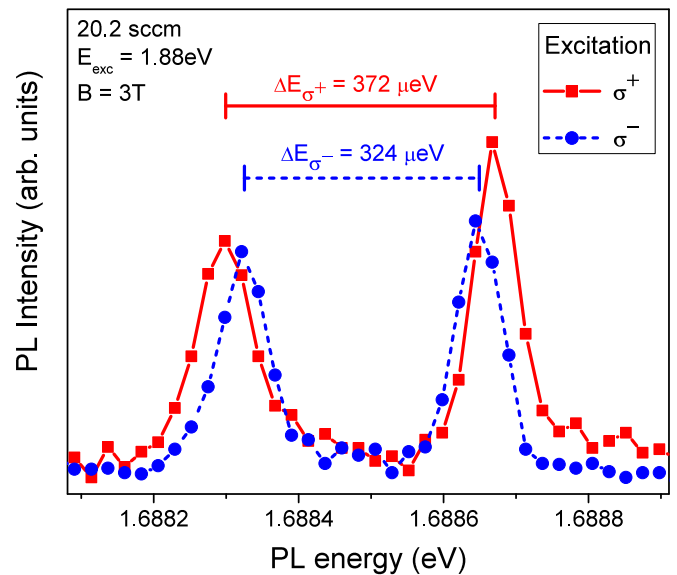


FIG. 7. Photoluminescence spectra of an individual InAsP/GaInP quantum dot (20.2-sccm sample) measured under σ^+ (red solid line and squares) and σ^- (blue dashed line and circles) circularly polarized optical excitation at $B = 3.0$ T in Faraday geometry. Variation of the Zeeman doublet splitting ΔE_{σ^\pm} in the trion spectra measured under σ^\pm excitation reveals dynamic nuclear spin polarization. The Overhauser shift for this measurement is estimated to be $E_{\text{OHS}} = (\Delta E_{\sigma^+} - \Delta E_{\sigma^-})/2 \approx 24 \mu\text{eV}$. The Zeeman splittings ΔE_{σ^+} and ΔE_{σ^-} are shown by the horizontal bars.

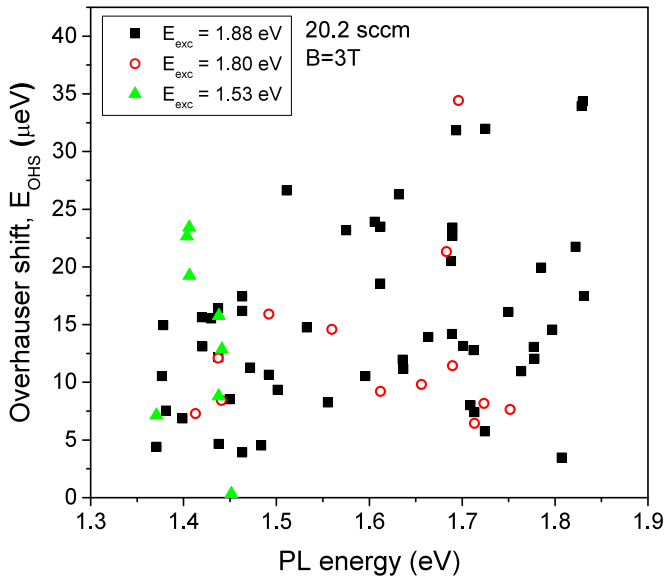


FIG. 8. Overhauser shifts measured in InAsP/GaInP quantum dots (20.2 sccm sample) at $B = 3$ T using circularly polarized excitation with three different photon energies: $E_{\text{exc}} = 1.88$ (squares), 1.80 (circles), and 1.53 eV (triangles).

spectra of the same InAsP/GaInP quantum dot are shown for σ^+ (squares) and σ^- (circles) excitation at $B = 3$ T. Gaussian fitting is used to determine the corresponding Zeeman splittings ΔE_{σ^+} , ΔE_{σ^-} (shown by the horizontal bars). The Overhauser energy shift E_{OHS} can be quantified by the difference between the Zeeman splitting ΔE observed when the nuclei are polarized and the splitting ΔE corresponding to zero nuclear polarization ($E_{\text{OHS}} = 0$). Realizing the $E_{\text{OHS}} = 0$ condition is demanding, so it is more practical to estimate the Overhauser shift as $E_{\text{OHS}} \approx (\Delta E_{\sigma^+} - \Delta E_{\sigma^-})/2$. This equation gives a lower bound estimate which is exact in case σ^\pm excitation produces E_{OHS} of the same magnitude but of the opposite signs. For the measurement presented in Fig. 7 we find $E_{\text{OHS}} \approx 24 \mu\text{eV}$.

Measurements of the Overhauser shifts were repeated at $B = 3$ T on a set of individual InAsP quantum dots emitting in a wide range of energies 1.3–1.8 eV as shown in Fig. 8. Circularly polarized excitation with different photon energies E_{exc} was employed. Excitation at $E_{\text{exc}} = 1.88$ eV (squares) is in resonance with the low-energy tail of the GaInP barrier, and was previously used to induce DNP in InP/GaInP QDs [28,44]. In addition, we used $E_{\text{exc}} = 1.80$ (circles) and 1.53 eV

(triangles) to study DNP in QDs emitting at lower energies. DNP with comparable Overhauser shifts E_{OHS} is observed for all E_{exc} used here. Overall, larger E_{OHS} is observed for InAsP dots with larger emission energy that are more reminiscent of InP dots. Nevertheless, the largest $E_{\text{OHS}} \approx 35 \mu\text{eV}$ observed here for InAsP dots is significantly smaller than in InP dots, where E_{OHS} exceeding $120 \mu\text{eV}$ has been achieved [45]. Since P and As have similar nuclear magnetic moments, such a reduction of E_{OHS} implies smaller degree of the optically induced nuclear spin polarization in the InAsP dots. On the other hand, such reduction in DNP efficiency agrees with our hypothesis about the type-II nature of the studied dots: longer exciton lifetimes can create a bottleneck and lower the efficiency of the cyclic nuclear spin polarization process [37,38,45]. Despite the smaller E_{OHS} values, observation of pronounced DNP opens the way for future studies using optically detected nuclear magnetic resonance (NMR) spectroscopy [48–52], which can provide further insights into chemical composition and strain profiles in the studied InAsP/GaInP quantum dots.

IV. CONCLUSIONS

We have presented a detailed study of individual InAsP/GaInP quantum dots in samples with different arsenic content grown by MOVPE. Our samples show QD emission in a broad optical spectral range (1.3 to 1.8 eV), confirming successful incorporation of arsenic into the dots. The combined analysis of the results of the electron microscopy imaging, exciton diamagnetic shifts and carrier g -factor measurements suggests that the studied InAsP/GaInP dots exhibit a type-II carrier confinement, where holes are localized in the InAs-rich core, while electrons reside in the InP-rich cap region. These properties make InAsP quantum dots of interest for efficient solar cell applications. Future work will include direct investigation of the type-II confinement by probing electron-hole recombination dynamics as well as further structural studies assisted by optically detected nuclear magnetic resonance techniques.

ACKNOWLEDGMENTS

This work has been supported by the EPSRC Programme Grant EP/J007544/1. O.D.P.-Z. and J.P. gratefully acknowledge the support from CONACYT-Mexico Doctoral Scholarship programme. E.A.C. was supported by a University of Sheffield Vice-Chancellor’s Fellowship and a University Research Fellowship from Royal Society.

[1] D. Bimberg and U. W. Pohl, *Materials Today* **14**, 388 (2011).
 [2] *Self-Assembled InGaAs/GaAs Quantum Dots*, edited by M. Sugawara, Semiconductors and Semimetals Vol. 60 (Academic Press, San Diego, 1999).
 [3] D. Bimberg and N. Kirstaedter, *IEEE Sel. Top. Quantum Electron.* **3**, 196 (1997).

[4] J. Shumway, A. J. Williamson, A. Zunger, A. Passaseo, M. DeGiorgi, R. Cingolani, M. Catalano, and P. Crozier, *Phys. Rev. B* **64**, 125302 (2001).
 [5] D. A. Vinokurov, V. A. Kapitonov, O. V. Kovalenkov, D. A. Livshits, and I. S. Tarasov, *Tech. Phys. Lett.* **24**, 623 (1998).
 [6] S. Fuchi, S. Miyake, S. Kawamura, W. Lee, T. Ujihara, and Y. Takeda, *J. Cryst. Growth* **310**, 2239 (2008).

- [7] E. Ribeiro and R. Maltez, *Appl. Phys. Lett.* **81**, 2953 (2002).
- [8] R. Maltez and E. Ribeiro, *J. Appl. Phys.* **94**, 3051 (2003).
- [9] I. Karomi, P. M. Smowton, S. Shutts, A. B. Krysa, and R. Beanland, *Opt. Express* **23**, 27282 (2015).
- [10] A. Krysa, J. Roberts, J. Devenson, R. Beanland, I. Karomi, S. Shutts, and P. Smowton, *J. Phys.: Conf. Ser.* **740**, 012008 (2016).
- [11] D. Dalacu, K. Mnaymneh, J. Lapointe, X. Wu, P. J. Poole, G. Bulgarini, V. Zwiller, and M. E. Reimer, *Nano Lett.* **12**, 5919 (2012).
- [12] H. Kosaka and A. Kiselev, *Electron. Lett.* **37**, 464 (2001).
- [13] J. van Bree, A. Y. Silov, P. M. Koenraad, M. E. Flatté, and C. E. Pryor, *Phys. Rev. B* **85**, 165323 (2012).
- [14] B. J. Witek, R. W. Heeres, U. Perinetti, E. P. A. M. Bakkers, L. P. Kouwenhoven, and V. Zwiller, *Phys. Rev. B* **84**, 195305 (2011).
- [15] S. Kim, B. Fisher, H.-J. Eisler, and M. Bawendi, *J. Am. Chem. Soc.* **125**, 11466 (2003).
- [16] R. B. Laghumavarapu, A. Moscho, A. Khoshakhlagh, M. El-Emawy, L. F. Lester, and D. L. Huffaker, *Appl. Phys. Lett.* **90**, 173125 (2007).
- [17] Z. Ning, H. Tian, C. Yuan, Y. Fu, H. Qin, L. Sun, and H. Ågren, *Chem. Commun.* **47**, 1536 (2011).
- [18] T. Tayagaki and T. Sugaya, *Appl. Phys. Lett.* **108**, 153901 (2016).
- [19] I. Kegel, T. H. Metzger, A. Lorke, J. Peisl, J. Stangl, G. Bauer, J. M. García, and P. M. Petroff, *Phys. Rev. Lett.* **85**, 1694 (2000).
- [20] D. Gerthsen, H. Blank, D. Litvinov, R. Schneider, A. Rosenauer, T. Passow, A. Grau, P. Feinäugle, H. Kalt, C. Klingshirn, and M. Hetterich, *J. Phys.: Conf. Ser.* **209**, 012006 (2010).
- [21] S. Yoon, Y. Moon, T.-W. Lee, E. Yoon, and Y. D. Kim, *Appl. Phys. Lett.* **74**, 2029 (1999).
- [22] S. Adachi, *J. Appl. Phys.* **53**, 8775 (1982).
- [23] M. D. Dawson and G. Duggan, *Phys. Rev. B* **47**, 12598 (1993).
- [24] C. J. Elliott, E. A. Chekhovich, M. S. Skolnick, A. I. Tartakovskii, and A. B. Krysa, *J. Phys.: Conf. Ser.* **245**, 012093 (2010).
- [25] M. Bayer, G. Ortner, O. Stern, A. Kuther, A. Gorbunov, A. Forchel, P. Hawrylak, S. Fafard, K. Hinzer, T. Reinecke *et al.*, *Phys. Rev. B* **65**, 195315 (2002).
- [26] E. A. Chekhovich, M. N. Makhonin, J. Skiba-Szymanska, A. B. Krysa, V. D. Kulakovskii, M. S. Skolnick, and A. I. Tartakovskii, *Phys. Rev. B* **81**, 245308 (2010).
- [27] B. Gotschy, G. Denninger, H. Obloh, W. Wilkening, and J. Schnieder, *Solid State Commun.* **71**, 629 (1989).
- [28] E. A. Chekhovich, A. B. Krysa, M. S. Skolnick, and A. I. Tartakovskii, *Phys. Rev. B* **83**, 125318 (2011).
- [29] S. N. Walck and T. L. Reinecke, *Phys. Rev. B* **57**, 9088 (1998).
- [30] L. M. Roth, B. Lax, and S. Zwerdling, *Phys. Rev.* **114**, 90 (1959).
- [31] A. A. Sirenko, T. Ruf, M. Cardona, D. R. Yakovlev, W. Ossau, A. Waag, and G. Landwehr, *Phys. Rev. B* **56**, 2114 (1997).
- [32] I. A. Yugova, A. Greilich, D. R. Yakovlev, A. A. Kiselev, M. Bayer, V. V. Petrov, Y. K. Dolgikh, D. Reuter, and A. D. Wieck, *Phys. Rev. B* **75**, 245302 (2007).
- [33] M. Syperek, D. R. Yakovlev, I. A. Yugova, J. Misiewicz, M. Jetter, M. Schulz, P. Michler, and M. Bayer, *Phys. Rev. B* **86**, 125320 (2012).
- [34] I. Vurgaftman, J. R. Meyer, and L. R. Ram-Mohan, *J. Appl. Phys.* **89**, 5815 (2001).
- [35] P. Lawaetz, *Phys. Rev. B* **4**, 3460 (1971).
- [36] M. Grundmann, O. Stier, and D. Bimberg, *Phys. Rev. B* **52**, 11969 (1995).
- [37] E. A. Chekhovich, M. N. Makhonin, A. I. Tartakovskii, A. Yacoby, H. Bluhm, K. C. Nowack, and L. M. K. Vandersypen, *Nat. Mater.* **12**, 494 (2013).
- [38] B. Urbaszek, X. Marie, T. Amand, O. Krebs, P. Voisin, P. Maletinsky, A. Högele, and A. Imamoglu, *Rev. Mod. Phys.* **85**, 79 (2013).
- [39] A. Abragam, *The Principles of Nuclear Magnetism* (Oxford University Press, London, 1961).
- [40] E. A. Chekhovich, A. Ulhaq, E. Zallo, F. Ding, O. G. Schmidt, and M. S. Skolnick, *Nat. Mater.* (2017), doi:10.1038/nmat4959.
- [41] D. Gammon, A. L. Efros, T. A. Kennedy, M. Rosen, D. S. Katzer, D. Park, S. W. Brown, V. L. Korenev, and I. A. Merkulov, *Phys. Rev. Lett.* **86**, 5176 (2001).
- [42] B. Eble, O. Krebs, A. Lemaître, K. Kowalik, A. Kudelski, P. Voisin, B. Urbaszek, X. Marie, and T. Amand, *Phys. Rev. B* **74**, 081306 (2006).
- [43] J. Puebla, E. A. Chekhovich, M. Hopkinson, P. Senellart, A. Lemaître, M. S. Skolnick, and A. I. Tartakovskii, *Phys. Rev. B* **88**, 045306 (2013).
- [44] J. Skiba-Szymanska, E. A. Chekhovich, A. E. Nikolaenko, A. I. Tartakovskii, M. N. Makhonin, I. Drouzas, M. S. Skolnick, and A. B. Krysa, *Phys. Rev. B* **77**, 165338 (2008).
- [45] E. A. Chekhovich, M. N. Makhonin, K. V. Kavokin, A. B. Krysa, M. S. Skolnick, and A. I. Tartakovskii, *Phys. Rev. Lett.* **104**, 066804 (2010).
- [46] E. A. Chekhovich, A. B. Krysa, M. S. Skolnick, and A. I. Tartakovskii, *Phys. Rev. Lett.* **106**, 027402 (2011).
- [47] P. Fallahi, S. T. Yilmaz, and A. Imamoglu, *Phys. Rev. Lett.* **105**, 257402 (2010).
- [48] E. A. Chekhovich, K. V. Kavokin, J. Puebla, A. B. Krysa, M. Hopkinson, A. D. Andreev, A. M. Sanchez, R. Beanland, M. S. Skolnick, and A. I. Tartakovskii, *Nat. Nanotechnol.* **7**, 646 (2012).
- [49] E. A. Chekhovich, M. Hopkinson, M. S. Skolnick, and A. I. Tartakovskii, *Nat. Commun.* **6**, 6348 (2015).
- [50] E. A. Chekhovich, M. M. Glazov, A. B. Krysa, M. Hopkinson, P. Senellart, A. Lemaître, M. S. Skolnick, and A. I. Tartakovskii, *Nat. Phys.* **9**, 74 (2013).
- [51] M. Munsch, G. Wust, A. V. Kuhlmann, F. Xue, A. Ludwig, D. Reuter, A. D. Wieck, M. Poggio, and R. J. Warburton, *Nat. Nanotechnol.* **9**, 671 (2014).
- [52] A. M. Waeber, M. Hopkinson, I. Farrer, D. A. Ritchie, J. Nilsson, R. M. Stevenson, A. J. Bennett, A. J. Shields, G. Burkard, A. I. Tartakovskii, M. S. Skolnick, and E. A. Chekhovich, *Nat. Phys.* **12**, 688 (2016).